Ignition and Charring of PVC-Based Electric Cables

Romain Meinier, Mahdi Fellah, Rodolphe Sonnier, Pascal Zavaleta, Sylvain Suard, Laurent Ferry

▶ **To cite this version:**

HAL Id: hal-03335336

https://imt-mines-ales.hal.science/hal-03335336

Submitted on 1 Jun 2022

Ignition and Charring of PVC-Based Electric Cables

Romain Meinier and Mahdi Fellah, Polymers Composites and Hybrids (PCH), IMT Mines Ales, 30319 Ales, France and Institut de Radioprotection et de Sûreté Nucléaire (IRSN), PSN-RES, SA2I, LEF, Cadarache, 13115 St Paul-Lez-Durance Cedex, France

Rodolphe Sonnier ID*, Polymers Composites and Hybrids (PCH), IMT Mines Ales, 30319 Ales, France

Pascal Zavaleta and Sylvain Suard, Institut de Radioprotection et de Sûreté Nucléaire (IRSN), PSN-RES, SA2I, LEF, Cadarache, 13115 St Paul-Lez-Durance Cedex, France

Laurent Ferry, Polymers Composites and Hybrids (PCH), IMT Mines Ales, 30319 Ales, France

Abstract. The ignition of four different PVC-based electric cables was studied using cone calorimeter and the influence of the charring phenomenon on ignition was investigated. The thermophysical and optical properties of the sheaths before decomposition were measured. The kinetics of charring was studied by photogrammetry. It was shown that charring occurs for three cables before ignition at heat flux lower than 45 kW/m². The lower is the heat flux, the higher is the char amount at ignition. In spite of the char formation, it was observed that the time-to-ignition of the cables can be properly calculated using the well-known Quintiere's equation, considering an apparent temperature of ignition. This apparent temperature at ignition was found in the range 312°C to 349°C for the four electric cables.

List of Symbols

c	Specific heat (J/(kg.K))
CHF	Critical heat flux (kW/m²)
D	Thermal diffusivity (m²/s)
h	Heat exchange coefficient (W/(m² K))
HF	External heat flux (W/m²)
I	Spectral emittance (W m⁻² m⁻¹)
k	Thermal conductivity (W/(m K))
L	Sample thickness (m)
R	Reflectance (-)
T_0	Initial temperature (K)

*Correspondence should be addressed to: ; Rodolphe Sonnier, E-mail: rodolphe.sonnier@mines-ales.fr

T_{ig} Surface temperature at ignition (K)
T_p Temperature of the first peak of mass loss rate (K)
TTI   Time-to-ignition (s)
t   Time (s)
t_{char} Time for char appearance (s)
TRP   Thermal Response Parameter (kW $s^{1/2}$ m^{-2})
V_{char} Char volume (cm^3)
XLPE   Crosslinked polyethylene

Greek symbols

α Absorbance (-)
ε Emissivity (-)
λ Wavelength (m)
σ Stefan-Boltzmann constant (5.67×10^{-8} Wm^{-2} K^{-4})
ρ Density (kg/m^3)

1. Introduction

Electrical cables make up the largest amount of combustible material present in Nuclear Power Plants (NPPs) and therefore contribute significantly to fire hazard in such facilities [1]. In order to assess this hazard, cable flammability has been extensively studied for a long time. Nevertheless, in their recent comprehensive review, Huang and Nakamura note that great efforts remain to be carried out to better understand the flame spread in case of multiple cables, as cable trays, due to interactions between them [2]. For example, Huang et al. have compared the flame spread on vertical cable trays with different arrangements (0 or 8 mm spacing between cables). They found that the flame spread is much faster when spacing is 8 mm [3].

Among the approaches to predict the flame spread on cable trays, the FLASH-CAT model was developed for horizontal ladder cable trays. Input of this model includes thermophysical properties of the cables but also some important fire parameters measured at small-scale, including the time-to-ignition [4].

Cone calorimeter is the most popular apparatus to study the fire behaviour at bench scale. Works have already been carried out to correlate the fire performance of cable trays at full scale with cone calorimeter results [5]. Especially due to the simple geometry of the test, relations between the time-to-ignition (TTI) and the temperature of the upper surface (T) in cone calorimeter have been proposed (Eqs. 1 and 2) assuming that ignition occurs when the surface temperature of the sample reaches the so-called ignition temperature T_{ig}. Note that these Equations were proposed for flat samples.

Time-to-ignition for thermally thick materials can then be predicted using Eq. 1 [6].

$$TTI = \frac{\frac{2}{3} \times k\rho c \times \left(T_{ig} - T_0\right)^2}{\left(\varepsilon \times HF - h\left(T_{ig} - T_0\right) - \varepsilon\sigma T_{ig}^4\right)^2} \tag{1}$$

where *HF* is the external incident radiative heat flux (W/m^2), T_0 the initial surface temperature (K), *k* the thermal conductivity (W/(m.K)), ρ the density (kg/m^3), *c* the specific heat (J/(kg.K)), ε the emissivity, *h* the heat exchange coefficient (W/(m^2.K)) and σ the Stefan Boltzmann constant.

Equation 2 was proposed for thermally thin materials [7].

$$TTI = \frac{L\rho c \times \left(T_{ig} - T_0\right)}{\left(\varepsilon \times HF - h\left(T_{ig} - T_0\right) - \varepsilon\sigma T_{ig}^4\right)} \tag{2}$$

where L (m) is the thickness of the sample.

Lyon and Quintiere have listed the ignition temperature for many pure polymers [8]. Ignition temperature mainly depends on materials but is relatively independent on heat flux [8, 9]. On the contrary, thermophysical properties change continuously with temperature, i.e. when the material is heated. Nevertheless, it has been shown that Eq. 1 allows the times-to-ignition to be calculated properly by considering the thermophysical properties at room temperature (i.e. without taking into account their change due to heating). More precisely, the product $k\rho c$ is supposed constant in Eq. 1 [6, 10].

Different authors have questioned the reliability of the Eqs. 1 and 2 and their limits. Especially, these models fail to predict accurately the time-to-ignition when in-depth absorption is not negligible [11]. For example, time-to-ignition of clear PMMA (poly(methyl methacrylate)) is significantly different in different fire apparatus because its heat absorption is strongly dependent on the emission spectrum of the source: electrical cone heater or tungsten lamps [12]. Below 2 μm, heat transmission is significant for this polymer [13]. In PDMS (polydimethylsiloxane) filled with very low content of multiwall carbon nanotubes, in-depth absorption was also found to monitor the time-to-ignition [14]. Inaccurate predictions are also found when thermo-physical or thermo-optical properties change during heating. Sonnier et al. have studied LDPE (low density polyethylene) samples coated with semi-opaque to opaque LDPE films containing aluminium particles [15]. In some cases, they showed that TTI can be well predicted but considering a lower emissivity than expected because the aluminium particles accumulate gradually as LDPE is degraded during pre-ignition. Time-to-ignition of PEEK (polyether ether ketone) in cone calorimeter is also modified in presence of a very small amount of moisture in the polymer due to surface bubble formation leading to a change in thermo-optical properties [16].

Concerning cables, two halogen-free flame retardant cables were studied by Meinier et al. [17]. It was shown that these cables behaved as thermally thick materials, and times-to-ignition were accurately predicted using the thermophysical properties of the cable sheath, measured at room temperature.

PVC-based electric cables were excluded from this first study, due to the occurrence of an additional phenomenon before ignition, namely charring. Indeed, when charring occurs before ignition, it is obvious that the above approximation (namely the constancy of the product $\lambda\rho c$) can no longer be considered reliable.

The char expansion (intumescence) may limit the pyrolysis surface exposed to heat flux and reduce the heat transmitted by heat conductivity to the underlying material. Therefore, the prediction of time-to-ignition for such cables remains unsolved. Gong et al. have studied the spontaneous ignition of a cable based on a PVC outer sheath and a crosslinked polyethylene (XLPE) insulation with a special device [18]. They observed that the PVC sheath swells and shrinks through five stages. The authors concluded that the pyrolysis gases from XLPE insulation are ignited by smoldering hot spot on charring PVC sheath. They did not attempt to predict TTI taking into account the thermophysical properties of the materials.
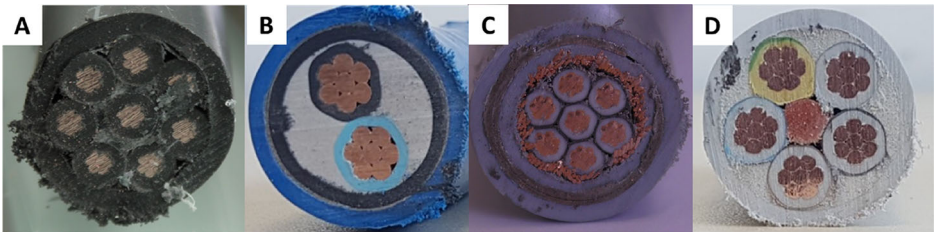
The present article investigates in details the pre-ignition charring phenomenon in PVC cables and its impact of their piloted TTI. Moreover, the reliability of the Quintiere's model for ignition (Eq. 1) in the context of charring materials is discussed. The objective is to check if TTI of such cables may be still properly assessed despite the early formation of the intumescent charring layer from the decomposition of external sheath. Providing accurate TTI analytical expression as inputs for FLASH-CAT or other numerical models would be useful in order to predict the development of cable trays fire.

2. Materials and Methods

Four PVC-based electric cables commonly found in NPPs [19, 20] are considered in this study. They differ from their structure, geometry and composition. They are labelled by a letter (A, B, C, D) followed by their diameter in mm. Cable A14 has been studied in details in a previous article [21]. A picture of their section is shown in Fig. 1. Cable structures are described in Table 1.

2.1. Thermophysical Properties of Sheath Materials

Thermophysical properties were measured at room temperature on sheath materials. Density, ρ (kg/m^3), was assessed using a helium Pycnometer (Micromeritics AccuPyc 1330). Specific heat, c (J/kg.K), was measured using a Perkin Elmer differential scanning calorimetry (Stepscan software). The measurement of heat diffusivity, D (m^2/s), was carried out using a Laser Flash apparatus (XFA600 from Linseis). Sheaths were cut from cables and flattened by thermocompression at 170°C under 50 bars during 5 min within a 4 mm thick square mould. Samples

Figure 1. Structure of the four cables tested in this study (a–Cable A14, b–Cable B29, c–Cable C16, d–Cable D28).

Table 1
Characteristics of the Four Electric Cables

	Cable A14	Cable B29	Cable C16	Cable D28
Cable diameter (mm)	14	29	16	28
Sheath thickness (mm)	1.5	2	1.3	2
Linear density (kg/m)	0.33	1.52	0.43	2.00
Sheath mass fraction	0.29	0.15	0.21	0.14
Copper mass fraction	0.44	0.39	0.18	0.59
Shield	No	Yes	Yes	No

were stamped from flat sheets and were coated with graphite on both surfaces. Measurements were carried out in vacuum. Values were averaged over five measurements. Thermal conductivity k, was calculated according to the Eq. 3:

$$k = D \times \rho \times c \tag{3}$$

2.2. Emissivity of Sheath Materials

Hemispherical spectral reflectance of sheath $R(\lambda)$ was measured in the wavelength range from $\lambda_1 = 0.4$ µm to $\lambda_2 = 22.2$ µm. Four wavelength ranges were used: [1.67 µm to 22 µm]: Infragold® integrating sphere, KBr beamsplitter, Globar source, HgCdTe detector; [0.91 µm to 2.22 µm], spectralon® integrating sphere, CaF_2 beamsplitter, halogen source, InGaAs detector; [0.67µm to 1.11 µm], spectralon integrating sphere, CaF_2 beamsplitter, halogen source, Silicon detector. For these three ranges, a Bruker® Vertex 80 V® IRTF spectrometer was used. The last spectral range [0.4 µm to 0.8 µm] was covered by using a Cary 500® grating spectrometer with a spectralon integrating sphere. Spectral absorbance $\alpha(\lambda)$ was calculated as $1 - R(\lambda)$ assuming that sheaths are opaque materials. In order to determine the absorbance α, which corresponds to the part of the heat flux emitted by the source which is absorbed by the material, the radiant cone was considered as a blackbody. The temperature of the equivalent black emitter T_{bb} for the different tested heat fluxes was chosen according to the values obtained by Boulet et al. [12, 22] and varies from 840 K for a heat flux of 20 kW/m² to 1450 K for a heat flux of 80 kW/m². α was then calculated as follows (Eq. 4):

$$\times \alpha(T_{bb}) = \frac{\int_{\lambda_1}^{\lambda_2} I_{bb}(\lambda, T_{bb}) \times \alpha(\lambda) d\lambda}{\int_{\lambda_1}^{\lambda_2} I_{bb}(\lambda, T_{bb}) d\lambda} \tag{4}$$

where $I_{bb}(\lambda, T_{bb})$ is the spectral emittance (in W m⁻² m⁻¹) of the blackbody heated at temperature T_{bb}. Note that for opaque materials as the sheaths, the emissivity ε used in Quintiere's model is equal to the absorbance α.

2.3. Thermogravimetric Analysis

Thermogravimetric analyses (TGA) were carried out on sheath materials using a Setsys Evolution apparatus (Setaram). The samples (10 ± 2 mg) were heated under nitrogen flow (100 mL/min) at a heating rate equal to 1 K/s from room temperature to 900°C.

2.4. Cone Calorimeter Tests

Ignition was studied using a cone calorimeter (Fire Testing Technology) according to the ISO 5660 standard. Tests were carried out on the four electric cables at various heat fluxes (especially in the range 20 kW/m^2 to 45 kW/m^2 to highlight the influence of charring on ignition) in well-ventilated conditions (24 l/s) and in presence of a spark igniter to force ignition. The distance between the cone and the top of the cable section was fixed to 25 mm. One section of cable (10 cm long) was used for each test (for cables B29, C16 and D28). In order to check the influence of the amount of cables on ignition, tests with filled sample holder (the number of sections depends on the cable diameter) were also performed (see supporting information S1). The results show that the number of cables has no influence on TTI. For cable A14, tests were performed only with filled sample holder. Figure 2 shows the layout of cables when the sample holder is filled for white cable.

In order to study char formation in detail, some tests were interrupted before ignition, and the section of cables was carefully picked up for further analysis.
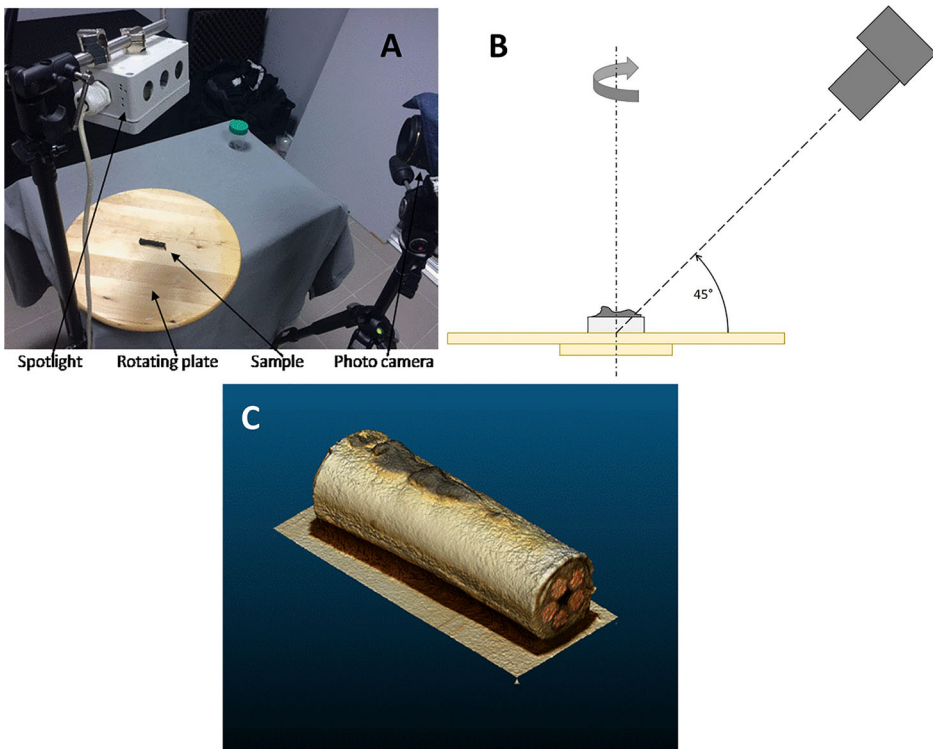

Figure 2.   Sample holder with cables D28 for cone calorimeter test.

2.5. Photogrammetry

The volume of the char formed on the cable was measured by photogrammetry. The whole cable exposed under the cone calorimeter is removed at a specific time. The removal of the char from the cable sample is a delicate operation. Therefore, the char is 3D reconstructed with the rest of the cable sample. Therefore, only the apparent volume of the char is being studied.

The cable sample with the formed char is then placed on a rotating plate. Afterwards, 36 pictures of the char were taken using a Nikon D850 as follows. The sample placed on the plate was shot every 10°. The artificial lightening is monitored because a difference between photos can prevent the parallax recognition. For that, a spotlight was installed above the sample to ensure the reconstruction without moving the camera. A reconstruction software (Agisoft PhotoScan) was used to isolate and generate an image of the char from the 36 pictures recorded. The device as well as an example of char volume rebuilt using this procedure is presented in Fig. 3.

Figure 3. Picture (a) and scheme (b) of device for photogrammetry measurement and example of rebuilt volume for the cable D28 (c).
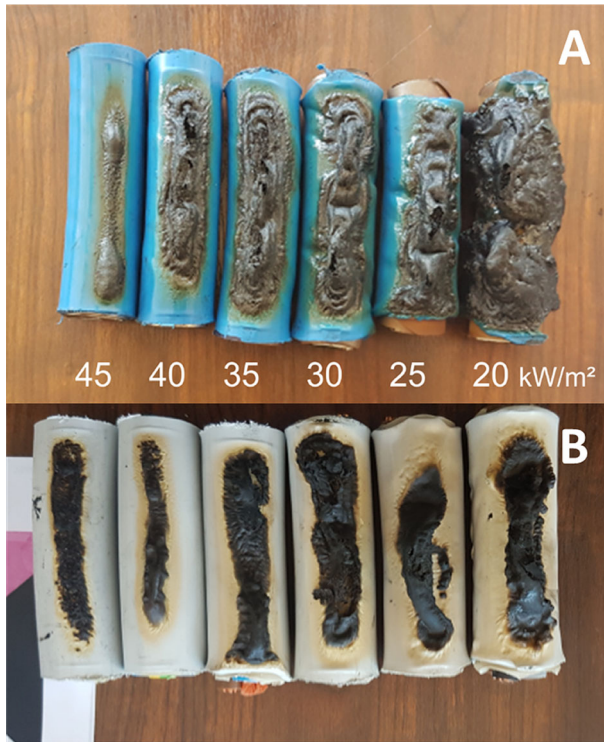
3. Results and Discussion

3.1. Times-to-Ignition of Cables and Char Appearance

Times-to-ignition of cables were recorded over a large range of heat fluxes and more especially at low to moderate heat flux because charring is clearly noticeable before ignition only for heat flux lower than 45 kW/m² (see an example in movie S2—Supporting information). Charring before ignition is very limited (almost negligible) for the cable A14. For the three other cables, the char amount is significant (see for example Fig. 4) even if it is higher for the cables B29 and C16 than for the cable D28. Note that charring is covering the surface at various rates according to cable (compare cables B29 and D28).

Times-to-ignition and times for char appearance (t_{char}, determined with naked eye) are listed in Table 2. Both times depend on heat flux according to a power law (exponent − 0.5), in agreement with the thermally thick behaviour expected for these cables (Fig. 5).

Critical heat flux for ignition has been calculated (by extrapolating the curve $TTI^{-0.5} = f(HF)$ to $TTI^{-0.5} = 0$) from data obtained for heat fluxes in the range 20 kW/m² to 45 kW/m²: its value is similar for the three charring cables (12 kW/

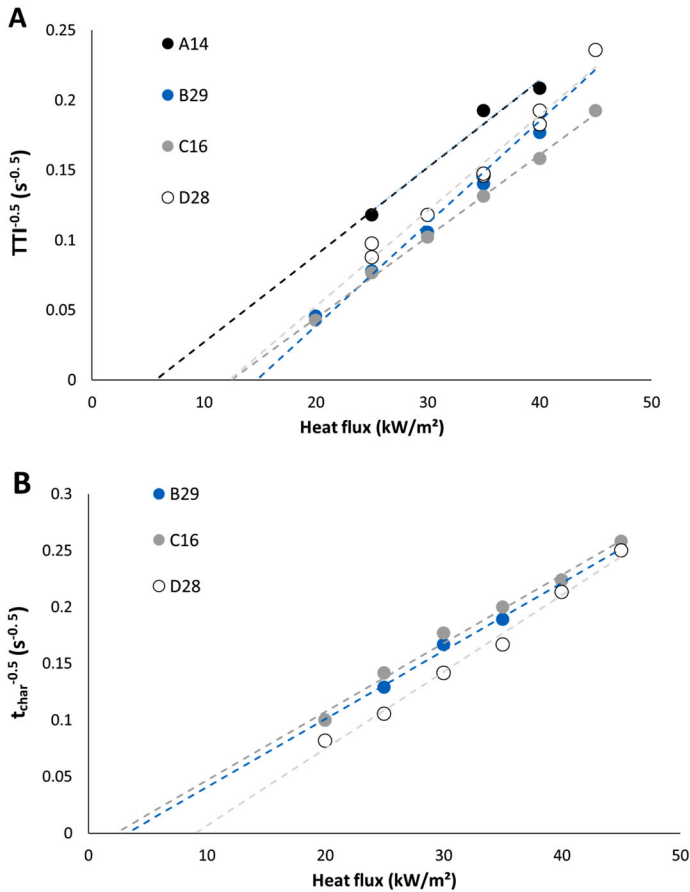**Figure 4.** Aspect of cables B29 (a) and D28 (b) at ignition for various heat fluxes.

Table 2
Times-to-Ignition and Temperatures of Char Appearance for Various Heat Fluxes

Heat flux (kW/m^2)	TTI (s)	t_{char} (s)	$\frac{TTI - t_{char}}{TTI}$
Cable A14			
25	72	–	–
35	27	–	–
40	23	–	–
55	12	–	–
70	6	–	–
80	4	–	–
Cable B29			
20	480	100	0.79
25	165	60	0.64
30	90	36	0.60
35	51	28	0.45
40	32	20	0.38
45	20	16	0.20
Cable C16			
20	560	100	0.82
25	170	50	0.71
30	96	32	0.67
35	58	25	0.57
40	40	20	0.50
45	27	15	0.44
Cable D28			
20	300	150	0.50
25	130	90	0.31
30	72	50	0.31
35	47	36	0.23
40	27	22	0.19
45	18	16	0.11

m^2 to 15 kW/m^2) but lower for cable A14 (6 kW/m^2). The critical heat flux for char appearance was also calculated (by extrapolating the curve $t_{char}^{-0.5} = f(HF)$ to $t_{char}^{-0.5} = 0$): its value is very low for cables B29 and C16 (2 kW/m^2 to 3 kW/m^2) and slightly higher for cable D28 (9 kW/m^2). All values are listed in Table 3.

Pre-ignition can be divided in two periods for cables B29, C16 and D28: the first period before charring (i.e. from 0 s to t_{char}) and the second period between char appearance and ignition (i.e. from t_{char} to TTI). The relative duration of this second period $(= \frac{TTI - t_{char}}{TTI})$ increases when heat flux decreases (see Table 2 and Figure S3 in supporting information). This second period is also relatively longer for cables B29 and C16, in comparison to cable D28.

Char volume has also been assessed at ignition by photogrammetry for the three cables at different heat fluxes (Fig. 6). It is clear that the char at ignition is more and more developed when heat flux decreases. Note that the measurement
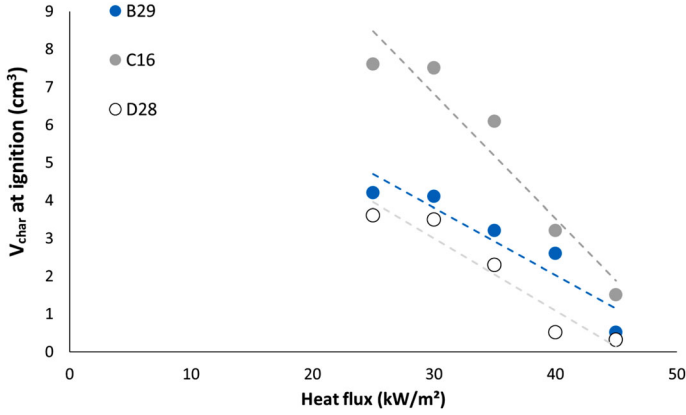
Figure 5. $\frac{1}{\sqrt{TTI}}$ (a) and $\frac{1}{\sqrt{t_{char}}}$ (b) versus heat flux.

Table 3
Critical Heat Fluxes for Ignition and Char Appearance

	Cable A14	Cable B29	Cable C16	Cable D28
CHF for ignition (kW/m^2)	6	15	13	12
CHF for char appearance (kW/m^2)	–	3	2	9

was not carried out at 20 kW/m^2 because the char cannot be properly separated from the remaining cable. Even if the relation between V_{char} and heat flux is not clearly linear, it is obvious that the char volume at ignition becomes null (or at least negligible) when the heat flux is higher than 45 kW/m^2 to 50 kW/m^2. Which-
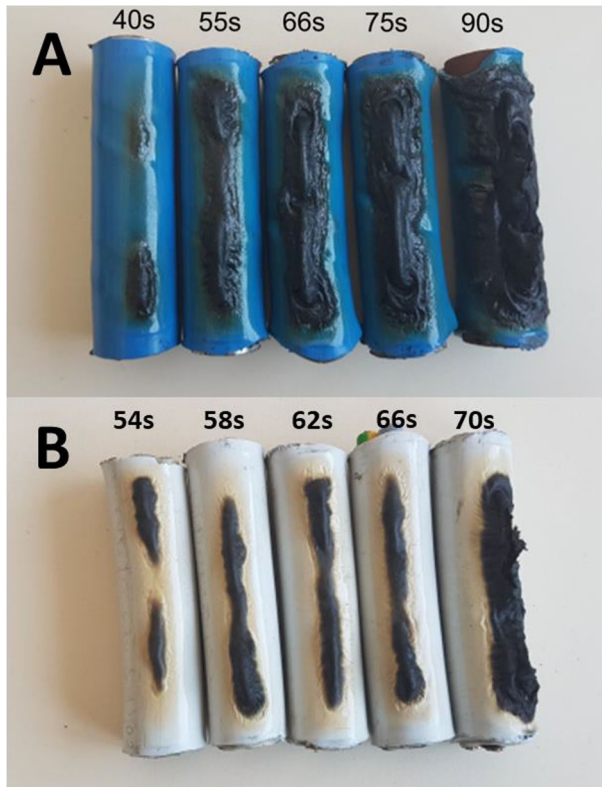
Figure 6. Char volume at ignition for various heat flux.

ever the heat flux, the char volume at ignition is the highest for cable C16 and the lowest for the cable D28.
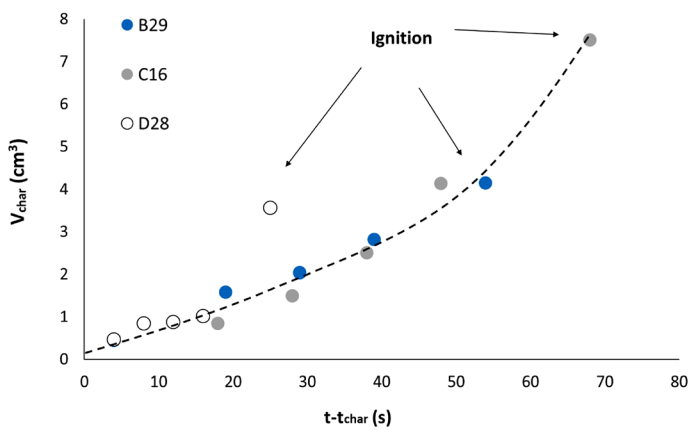
Cone calorimeter tests at 30 kW/m^2 were interrupted at various times before ignition and the volume of char was systematically measured using the procedure previously described. Figure 7 shows the aspect of cables B29 and D28 at various times. Figure 8 shows the change in char volume versus t-t$_{char}$, i.e. the time from which char is appearing (determined with the naked eye). This value t$_{char}$ is 36, 32 and 50 s respectively for cables B29, C16 and D28 at 30 kW/m^2. Except the final data point at ignition for cable D28, all the data points follow a same tendency. The increase rate of char volume is similar for the three cables. The highest amount of char at ignition for cable C16 is correlated to the longest period between char appearance and ignition. On the contrary, the low amount of char at ignition for cable D28 corresponds to earlier ignition.

As already noted from Fig. 4, the surface covering of the char seems to be different, higher for cables B29 (and C16) and lower for cable D28. Moreover, the char properties may influence its role to prevent heat transfer. The volume of char is probably not the only parameter to take into account to assess the role of char on ignition. Nevertheless, it would be expected that the pre-ignition charring may have a major effect on time-to-ignition.

As explained in the introduction part, the main motivation of this work is to assess if Eq. 1 given by [6] allows the time-to-ignition of PVC-based cables, measured in cone calorimeter, to be predicted in order to provide accurate inputs for numerical modelling. In the present configuration, the temperature on the upper surface is no longer homogeneous and therefore Eq. 1should not be effective. Indeed, both charred and uncharred surfaces exhibit two different temperatures and the volumes under these surfaces contribute to release pyrolysis gases. Moreover, the char modifies the heat transfer because its thermal conductivity, density and specific heat change from the values of initial material [23]. Finally, the char expands and its thickness contributes to thermal insulation.

Figure 7. Aspect of cables B29 (a) and D28 (b) at various times before ignition (heat flux 30 kW/m²).

Figure 8. Char volume versus t-t$_{char}$ for the three cables at 30 kW/m².

From a practical point of view, it may be still possible to find a set of values (k, c, ρ, ε, T_{ig}) which allows to calculate properly the TTI. These values would be only apparent ones. In the following, the thermophysical and thermo-optical properties (k, c, ρ, ε) will be kept constant to the initial values. Then, T_{ig} will be chosen to fit at best the TTIs measured on cables.

3.2. Thermophysical and Optical Properties of Sheaths

Thermophysical and thermo-optical properties of sheath materials for PVC-based cables are listed in Table 4. Emissivity is high in all cases as expected for polymers filled with various additives. Its value tends to decrease when heat flux increases (i.e. when the cone temperature increases). The highest value is found for cable A14. For this cable, the emissivity is almost independent on the heat flux. Thermal inertia ($\sqrt{c\rho k}$) is relatively similar for the four sheaths (531 W s$^{1/2}$/m^2 K to 704 W s$^{1/2}$/m^2 K), i.e. around 1.5 to 2 times less than halogen-free cables studied in our previous article ($\sim$ 1000 W s$^{1/2}$/m^2 K for cable A in [17]). This observation, as well as the significantly lower apparent temperature of ignition of PVC-based cables (see below) explain why these cables ignite much earlier. Note that cable A14 exhibits the lowest thermal inertia. It means that the surface temperature of this cable increases faster. Consequently, the temperature at ignition should be reached faster: this may explain why the charring seems not to develop before ignition. The delay between the appearance of char and the ignition is too short. Courty and Garo have investigated the piloted ignition of a PVC-based cable (diameter 1.5 cm). They found TTI comparable to those measured on cable A14 (around 44 s at 20 kW/m^2 and 25 s at 30 kW/m^2). The authors did not mention any charring before ignition for this cable, as for our own black cable [24].

Table 4
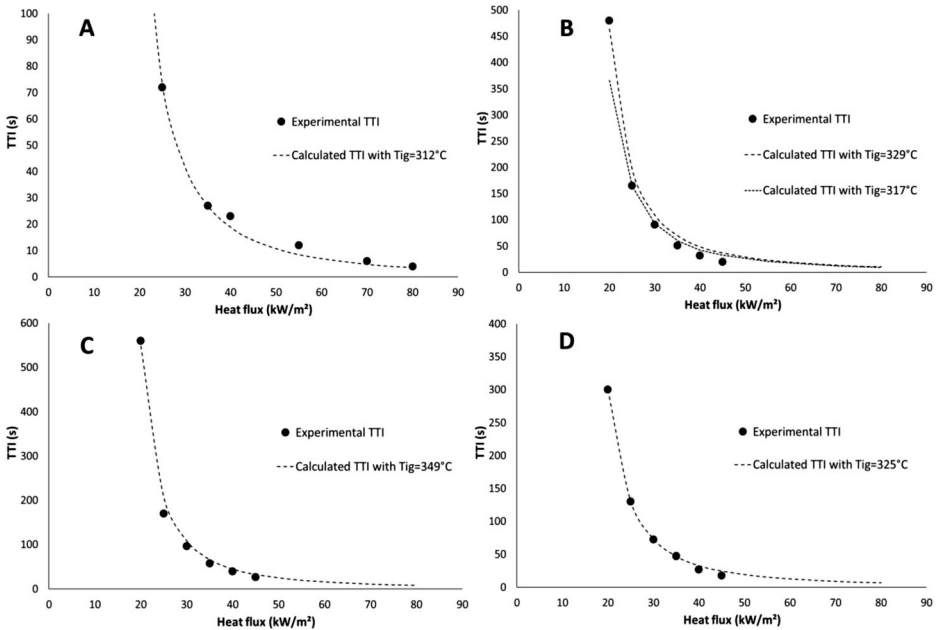**Thermophysical and Thermo-Optical Properties of Sheath Materials (Measured at Room Temperature)**

	Cable A14	Cable B29	Cable C16	Cable D28	HFFR Cable A in [17]
Specific heat c (J/kg.K)	1320	1282	1320	1110	1520
Density ρ (kg/m^3)	1336	1382	1483	1520	1540
Heat diffusivity (mm^2/s)	0.091	0.158	0.102	0.136	0.216
Heat conductivity k (W/ m K)	0.16	0.28	0.2	0.23	0.503
$\sqrt{c\rho k}$ (W s$^{1/2}$/m^2 K)	531	704	626	623	1085
Emissivity ε*	0.95 to 0.94	0.89 to 0.79	0.90 to 0.87	0.92 to 0.85	$\sim$ 1

*For heat flux ranged from 20 kW/m^2 to 80 kW/m^2

3.3. Determination of Apparent Temperature at Ignition for Cables

Times-to-ignition were calculated using Eq. 1 and choosing T_{ig} to minimize the difference between experimental and calculated TTI over the whole range of heat flux (see Figs. 9 and Table 5). From Figs. 9, it is clear that the choice of T_{ig} in the range 312°C to 349°C (depending on the cable) allows fitting accurately TTI over the whole range of heat flux. In other words, time-to-ignition can be accurately predicted using Eq. 1and considering a unique "apparent" T_{ig} for each cable (see Table 5). Predicted TTI are slightly less satisfying for cable B29 while they are systematically underevaluated by 15 s to 20 s. A temperature of 317 °C may allow a much better fit over the range 25 kW/m² to 45 kW/m², but a larger gap between experimental and calculated TTI at 20 kW/m². Figure 9b shows the calculated TTI for cable B29 using these two different temperatures at ignition (with T_{ig} = 329 or 317 °C). Note that there is no great change in the range 25 kW/m² to 45 kW/m².

The Thermal Response Parameter (TRP = $\sqrt{\frac{2}{3}c\rho k}(T_{ig} - T_0)$) can be calculated using this temperature at ignition (Table 5). The values are found in the range 127 kW s$^{1/2}$ m^{-2} to 178 kW s$^{1/2}$ m^{-2} in agreement with values in literature for PVC-based cables. Courty et al. deduced a TRP of 141 kW s$^{1/2}$ m^{-2} from the slope of the curve $TTI^{-0.5} = f(HF)$ [24]. Tewarson gives TRP values in the range

Figure 9. Experimental and calculated times-to-ignition versus heat flux for the four cables—a/Cable A14; b/Cable B29; c/Cable C16; d/Cable D28.

Table 5
Calculated Apparent Temperature at Ignition for Cables

	T_{ig} (°C)	Thermal response parameter (kW s$^{1/2}$ m^{-2})
Cable A14	312	127
Cable B29	329*	178**
Cable C16	349	168
Cable D28	325	155

*Or 317 °C alternatively
**Or 171 kW.s$^{1/2}$ m^{-2} alternatively

156 kW s$^{1/2}$ m^{-2} to 341 kW s$^{1/2}$ m^{-2} for similar PVC-based cables [25]. Cable A14 exhibits the lowest TRP value reflecting its ability to ignite faster.

3.4. Thermogravimetric Analysis of Cable Sheaths

The apparent temperatures at ignition are much lower than that found by Lyon and Quintiere in the case of pure PVC (395°C to 530°C) [8]. The reason is that PVC sheath contains high amount of volatile phthalates which are released in gas phase at low temperature. Indeed, in our previous work on the cable A14, it was found that PVC accounts for only 41% of the weight of the sheath, other components were dioctyl phthalates, calcium carbonate and lead-based stabilizers. Therefore, the flammability of these cables strongly depends on plasticizer and not only on PVC matrix [21]. Gong et al. have also obtained a high temperature at ignition (500°C) for a cable based on a PVC outer sheath [18]. Nevertheless, in their work, they studied specifically the spontaneous (not piloted) ignition. Spontaneous ignition occurs at much higher temperature than piloted one.

Hence, the decomposition profile of sheaths is quite complex. Thermogravimetric curves for the four sheaths are shown in Fig. 10. DTG curves are shown in Supporting Information (S4). It is obvious that the composition of the sheaths is different even if the same decomposition steps can be found. Relying on our previous paper [21], three decomposition steps can be identified in the range 250°C to 320°C, 400°C to 460°C and 700°C to 760°C but their intensity depends on the material. The first step can be assigned to the dechlorination of PVC as well as the decomposition/volatilization of the plasticizer. The first mass loss is clearly split in two steps in the case of cable B29 sheath. The mass loss corresponding to this main step differs from 40% (for sheath from cable D28) to more than 60% (for sheaths from cables A14 and B29). The second step is related to the decomposition of the main chain of PVC (polyenes). The temperature of the third step (if any) corresponds to the decomposition of a mineral additive as calcium carbonate. In a previous article, we have shown that calcium carbonate is present in sheath from cable A14 but it reacts at much lower temperature with PVC to form $CaCl_2$ [21]. Therefore, we assume that calcium carbonate should be present in higher amount in sheaths from cables C16 and D28 and a fraction of unreacted calcium carbonate decomposes at around 750°C. Note also that the residue con-

Figure 10. Thermogravimetric curves for the four sheaths (anaerobic pyrolysis).

tent at 800°C is in the range 19% to 36% depending on the sheath. It is higher for sheaths from cables C16 and D28 for which we suggest that they contain more calcium carbonate.

Despite these differences, it can be noted that the decomposition starts in the same range for the four sheaths. The temperature at the first peak of mass loss rate (T_p) is in the range 268°C to 308°C, which is roughly 40°C lower than the apparent T_{ig}. Therefore, even if there is no accurate correlation between the decomposition temperature and the apparent temperature at ignition, this last one is close to the temperature at with HCl and phthalates are released for all cables. It confirms that the combustion is probably driven by the ignition of phthalates while the heat of combustion is small for gases released by PVC during the first decomposition step.

4. Discussion

While the apparent temperature at ignition is in the same range for the four cables: 312°C to 349°C, it may be desirable to consider only one mean temperature for the four PVC-based cables (i.e. 329°C). The Figure S5 in supporting information shows how the calculated time-to-ignition changes when the mean temperature at ignition is considered. The error on time-to-ignition remains quite limited (except for cable C16 at 20 kW/m^2). Note that TTIs are significantly different between the four cables. Anyway, even if the apparent temperature at ignition is found to be similar, the difference between TTI for the different cables is due to their thermophysical and optical properties. Especially, if the cable A14 ignites faster than the other ones, it is especially due to its higher emissivity and lower thermal inertia. From a practical point of view, this result shows that it is possible to predict the TTI of an unknown PVC-based cable with a relative accu-

racy considering a temperature at ignition around 329°C and to provide suitable data for numerical modelling.

This is an apparent paradox: Quintiere's model remains suitable to predict the time-to-ignition in cone calorimeter. TTIs were correctly predicted by Quintiere's model using the thermophysical and optical properties measured at room temperature and an apparent temperature at ignition. Note that our approach mainly consists to fit experimental values by adjusting only one parameter: the "apparent" temperature at ignition. It does not mean that the other (thermophysical and optical) properties are unchanged during the test. It means that the resulting variation of all the material properties is fully captured by this parameter.

However, this parameter is very similar for all the cables studied (whether or not there is charring before ignition). Three cables are charring before ignition, namely B29, C16 and D28. Char obviously modifies the thermophysical and optical properties and changes the heating kinetics of the material. Nevertheless, for these three cables as for the fourth one (A14), the apparent temperature at ignition is in the same range.

This paradox could mean that pre-ignition char has no significant influence on ignition or it occurs too late. Another assumption is that there is a compensation effect in the change of the thermophysical or optical properties. The expected decrease in heat conductivity or density or the increase in emissivity due to charring may accelerate the heating rate of the top surface but the porous char (with low heat conductivity) could limit the heat transfer so that a smaller volume may be heated.

Nevertheless, there may be some indices of the influence of char on TTI. First, higher is the char volume at ignition (as shown in Fig. 8), higher is the temperature at ignition (T_{ig}). Non-charring A14 exhibits the lowest TTI while C16 shows the highest TTI and char volume. A second indication would concern the gap between the temperature of the first peak of mass loss rate (T_p) in TGA and T_{ig}. Of course, the heating in TGA and in cone calorimeter is different and then there is no reason that the T_{ig} corresponds closely to T_p. Nevertheless, it is clear that the ignition is produced by the combustion of gases released during this first decomposition step, especially plasticizers. T_p is 308°C for non-charring cable A14, i.e. very close to the apparent T_{ig} of this cable (312°C). For the three other cables, the gap between T_p and T_{ig} is significant. This gap reaches 30°C for the cable D28, 21°C–33°C for the cable B29 (depending on the choice of T_{ig}) and up to 82°C for the cable C16 which shows the highest ability to form char before ignition. The charring during pre-ignition may shift the T_{ig} towards higher temperatures.

5. Conclusion

The pre-ignition period of four PVC-based cables was investigated with a special emphasis on the char formation and its potential role on ignition. Char amount at various times and heat fluxes was measured using photogrammetry.

The thermophysical and thermo-optical properties at room temperature were measured and the thermal inertia was found to be significantly lower than halogen-free flame retardant cables. Together with a lower temperature at ignition, this explains why the ignition of PVC-based cables occurs much earlier.

Three cables are developing char to varying degrees when heat flux is lower than 45 kW/m^2 to 50 kW/m^2. Char amount at ignition increases when heat flux decreases. Nevertheless, for the four cables, times-to-ignition can be accurately predicted using Quintiere's equation and considering a unique "apparent" temperature at ignition for all the heat fluxes. This temperature at ignition varies in a narrow range, i.e. 312°C to 349°C whether or not the cables are charring before ignition. Considering a mean value (329°C) for the four cables allows to predict the TTI with a satisfying accuracy and provides suitable inputs for numerical simulations.

References

1. Zavaleta P, Hanouzet R, Beji T (2019) Improved assessment of fire spread over horizontal cable trays supported by video fire analysis. Fire Technol 55:233–255
2. Huang X, Nakamura Y (2020) A review of fundamental combustion phenomena in wire fires. Fire Technol 56:315–360
3. Huang X, Zhu H, Peng L, Zheng Z, Zeng W, Bi K, Cheng C, Chow W (2019) Thermal characteristics of vertically spreading cable fires in confined compartments. Fire Technol 55:1849–1875
4. McGrattan K, Lock A, Marsh N, Nyden M, Price M, Morgan AB, Galaska M, Schenck K (2010) Cable heat release, ignition, and spread in tray installations during fire (Christifire) Volume 1: Horizontal Trays, United States Nuclear Regulatory Commission, Washington DC
5. Coaker A, Hirschler M, Shoemaker C (1992) Rate of heat release testing for vinyl wire and cable materials with reduced flammability and smoke full-scale cable tray tests and small-scale tests. Fire Saf J 19:19–53
6. Rhodes BT, Quintiere JG (1996) Burning rate and flame heat flux for PMMA in a cone calorimeter. Fire Saf J 26:221–240

7. Quintiere JG (2001) The effects of angular orientation on flame spread over thin materials. Fire Saf J 36:291–312

8. Lyon R, Quintiere J (2007) Criteria for piloted ignition of combustible solids. Combust Flame 151:551–559

9. Schartel B, Hull R (2007) Development fire-retarded materials—interpretation of cone calorimeter data. Fire Mater 31:327–354

10. Hopkins D Jr, Quintiere JG (1996) Material fire properties and predictions for thermoplastics. Fire Saf J 26:241–268

11. Bal N, Rein G (2011) Numerical investigation of the ignition delay time of a translucent solid at high radiant heat fluxes. Combust Flame 158:1109–1116

12. Boulet P, Parent G, Acem Z, Collin A, Försth M, Bal N, Rein G, Torero J (2014) Radiation emission from a heating coil or a halogen lamp on a semitransparent sample. Int J Therm Sci 77:223–232

13. Girods P, Bal H, Biteau H, Rein G, Torero J (2011) Comparison of pyrolysis behavior results between the cone calorimeter and the fire propagation apparatus heat sources. Fire Saf Sci 10:889–901

14. Sonnier R, Bokobza L, Concha-Lozano N (2015) Influence of multiwall carbon nanotube (MWCNT) dispersion on ignition of poly(dimethylsiloxane)–MWCNT composites. Polym Adv Technol 26:277–286

15. Sonnier R, Ferry L, Gallard B, Boudenne A, Lavaud F (2015) Controlled emissivity coatings to delay ignition of polyethylene. Materials 8:6935–6949

16. Oztekin E, Crowley S, Lyon R, Stoliarov S, Patel P, Hull R (2012) Sources of variability in fire test data: a case study on poly(aryl ether ether ketone) (PEEK). Combust Flame 159:1720–1731

17. Meinier R, Sonnier R, Zavaleta P, Suard S, Ferry L (2018) Fire behavior of halogen-free flame retardant electrical cables with the cone calorimeter. J Hazard Mater 342:306–316

18. Gong T, Xie Q, Huang X (2018) Fire behaviors of flame-retardant cables part I: decomposition, swelling and spontaneous ignition. Fire Saf J 95:113–121

19. Zavaleta P, Suard S, Audouin L (2019) Cable tray fire tests with halogenated electric cables in a confined and mechanically ventilated facility. Fire Mater 43:543–560

20. Siemon M, Riese O, Forell B, Krönung D, Klein-Heßling W (2019) Experimental and numerical analysis of the influence of cable tray arrangements on the resulting mass loss rate and fire spreading. Fire Mater 43:497–513. https://doi.org/10.1002/fam.2689

21. Decimus A, Sonnier R, Zavaleta P, Suard S, Ferry L (2019) Study of gases released under incomplete combustion using PCFC–FTIR. J Therm Anal Calorim 138:753–763

22. Boulet P, Parent G, Acem Z, Rogaume T, Fateh T, Zaida J, Richard F (2012) Characterization of the radiative exchanges when using a cone calorimeter for the study of the plywood pyrolysis. Fire Saf J 51:53–60

23. Beyler C , Hirschler M (2002) Thermal decomposition of polymers, SFPE handbook of Fire Protection Engineering, 3rd edn, Section 1, Chapter 7. ISBN: 087765-451-4

24. Courty L, Garo JP (2017) External heating of electrical cables and auto-ignition investigation. J Hazard Mater 321:528–536

25. Tewarson A (2002) Generation of heat and chemical compound in fires, SFPE handbook of fire protection engineering, ISBN:087765-451-4, Third edition, Section three, Chapter 4